Phonon-coupling enhanced absorption of alloyed amorphous silicon for solar photovoltaics

Jedo Kim and Massoud Kaviany*
Department of Mechanical Engineering, University of Michigan, Ann Arbor, Michigan 48109-2125, USA
(Received 17 August 2010; published 6 October 2010)

Using the observed temperature dependence of *a*-Si:H photon absorption spectrum and the weak-phonon interaction second-order transition theory, phonon-coupling enhanced photon absorption is predicted for *a*-Si-Ge and *a*-Si-Sn alloys. The *ab initio* calculated electron and phonon properties of the alloyed amorphous phase show minimally altered electronic states and significant redshifted phonon energies. This phonon shift enhances the optical phonon-coupled photon absorption resulting in increased current generation near the optical band edge. We find that this enhancement favors low-energy optical-phonon modes, thus making the soft-bond forming Sn the choice alloying element.

DOI: 10.1103/PhysRevB.82.134205 PACS number(s): 88.40.hj, 31.15.A−, 63.20.dk, 71.23.Cq

I. INTRODUCTION

a-Si:H is a low-cost solar photovoltaic (SPV) material with low-energy conversion efficiency compared to *c*-Si.[1] Alloyed *a*-Si:H has not been among the next generation SPV materials because *a*-Si technology has been considered to be relatively mature and the abstruse carrier transport physics of random structures pose as obstacle.[2] Earlier studies explored this complex carrier transport kinetics and recent *ab initio* calculations have dealt with the origin of the Urbach tails.[3] First-principles calculations on *a*-Si is challenging due to absence of long-range order. However, studies have used periodic disordered cells with good results.[4–6] Despite the challenges, amorphous solids provide a unique opportunity for theoretical prediction of phonon properties because of absence of the selection rule, especially momentum conservation, due to loss of translational symmetry.[2] In addressing SPV efficiency improvements, the role of phonon has not been properly explored than in other photonic devices.[7]

Using *X* alloying of *a*-Si with a phonon-participation perspective on solar-energy conversion, we show by alloying, the electronic density of states D_e of *a*-Si_xX_{1-x} is minimally altered, and that there is enhancement in the second-order, phonon-coupled photon absorption due to lower phonon energy and enhanced phonon density of states D_p. We select group-IV element to avoid doping effects due to extra electrons or holes, focusing on elements known to form similar tetragonal structure as Si (e.g., Ge and Sn). Especially, for Sn forming soft bonds, it is predicted to significantly lower the phonon energy in the alloy and reduce the electronic band gap.[8,9] Also, as the mass mismatch increases the desired separation of the phonon peaks (similar to phonon band gaps) resembles highly mismatched crystals.[10] While Si-Sn crystal faces phase separation,[8] introduction of Sn into an amorphous phase Si can circumvent this problem. Here, *a*-Si is simulated with disordered 64-atom cells generated by the Wooten-Winer-Weaire method.[11] To simulate an *a*-Si-*X* alloy we replace the Si atoms with *X* atoms. We average over six different configurations of *X* atoms in *a*-Si structure. We use the Fermi's golden rule, the harmonic vibration, and the ground-state electronic and phonon calculations for this preliminary atomistic model which allows for the optimization of the alloy.

II. ABSORPTION COEFFICIENT OF *a*-Si:H

We begin by examining the absorption coefficient of *a*-Si:H, as shown as a function of photon energy in Fig. 1.[12] There exists a significant temperature dependence of the absorption spectrum near the optical band edge and the spectrum shows direct-bandlike behavior. In semiconductors, the majority of this temperature dependence is known to be the result of electron-lattice interaction[13] which makes the role of phonon important at finite temperatures. Still, the optical transitions of *a*-Si:H and the effect of disorder, thermal vibration, and hydrogen content have not yet been clarified.[14,15] However, strong experimental data and theoretical analysis show the band gap is strongly dependent on the hydrogen content and the band-to-band optical transition is dominated by indirect (phonon-coupled) transition similar to *c*-Si.[16,17] So, the direct-bandlike absorption behavior is explained by phonon coupling in the absence of the momentum-conservation rule. We decompose the absorption

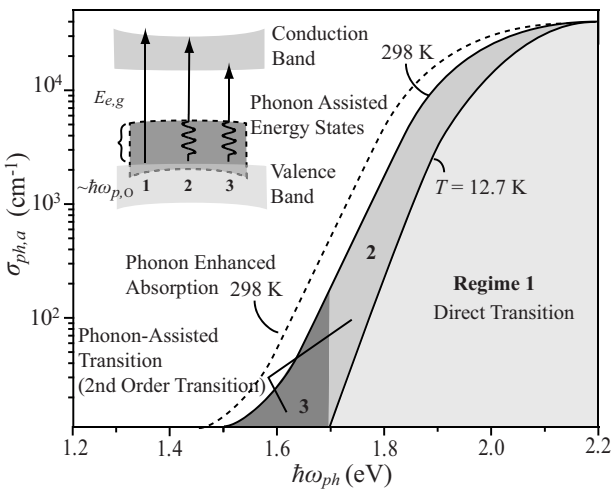

FIG. 1. Absorption coefficient for *a*-Si:H at 12.7 and 298 K (Ref. 12). At low temperatures, single-photon absorption is dominant but significant temperature dependence is shown near room temperature. The dotted line shows qualitative enhancement of absorption when the phonon coupling is enhanced with no temperature change. The inset shows the energy processes involved in the transitions.

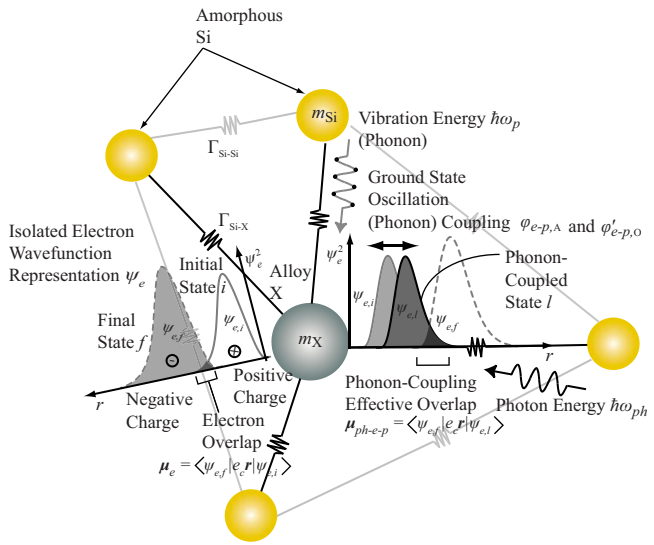

FIG. 2. (Color online) Conceptual rendering of photon-electron-phonon coupling in a-Si-X alloy using isolated electron representation. The electron distributions for initial (i), final (f), and phonon coupled (l) states are shown along with the photon and phonon energies.

coefficient into three distinct regimes, i.e., (1) direct absorption where only one photon is absorbed in the transition process, (2) phonon-assisted absorption where one phonon and one photon (with energy higher than the band gap) are absorbed, and (3) the same but for photon energy slightly lower than the band gap. When phonon-assisted absorption is enhanced, the absorption coefficient will increase at constant temperature, as shown by the dotted line. The electronic energy changes due to these processes are shown as an inset in Fig. 1 where phonon-assisted energy states appear due to electron-phonon interaction.

III. PHOTON-ELECTRON-PHONON INTERACTIONS AND ABSORPTION

Figure 2 renders conceptual photon-electron-phonon interaction in a-$Si_{1-x}X_x$. The initial i and final f are the semiconductor valence- and conduction-electron states. At $T>0$ phonons propagate through the lattice causing continuous excitation and de-excitation of electrons in the ground state. This interaction results in oscillation of the electrons through the acoustic and optical electron-phonon coupling $\varphi_{e\text{-}p,A}$ and $\varphi'_{e\text{-}p,O}$ and create the phonon-coupled energy states l.[18] These energy states contrast the strong-ion-coupled phonon states in isolated ions[19] since the electrons are not tightly bound to any ionized dopant. The a phase allows for an isolated electron wave function ψ_e representation, due to broken symmetry. Therefore, the interaction matrix can be expanded using the weak-phonon-coupling Hamiltonian, where the phonon-coupled states are treated as intermediate states during the transition. Then the electronic overlap (μ_e) turns into a phonon-coupling effective overlap ($\mu_{ph\text{-}e\text{-}p}$) which can be enhanced by alloy optimization.[20] When an electron is excited by absorption of a photon ($\hbar\omega_{ph}$), it leaves behind a positive charge (hole). This three carrier interaction can be represented by weak-phonon-coupled photon absorption (second-order transition) using Fermi's golden rule and is written as[21]

$$\dot{\gamma}_{ph\text{-}e\text{-}p} = \frac{2\pi}{\hbar}\sum_f |M_{ph\text{-}e\text{-}p}|^2 \delta_D(E_{e,f} - E_{e,i} - \hbar\omega_{ph} - \hbar\omega_p), \tag{1}$$

where δ_D is the Dirac delta, $E_{e,i}$, and $E_{e,f}$ are, respectively, the initial and final energies of the electron, and $\hbar\omega_{ph}=E_{ph}$ and $\hbar\omega_p=E_p$ are photon and phonon energies. $|M_{ph\text{-}e\text{-}p}|$ is the interaction matrix from a second-order perturbation theory and total Hamiltonian of the system is

$$H = H_e + H_p + H_{ph} + H_{ph\text{-}e} + H_{e\text{-}p}, \tag{2}$$

where H_e, H_p, H_{ph}, $H_{ph\text{-}e}$, and $H_{e\text{-}p}$ are electron, phonon, photon, electron-photon interaction, and electron-phonon interaction Hamiltonians, respectively. The acoustic and optical electron-phonon interaction can be written as

$$H_{e\text{-}p,A} = \varphi_{e\text{-}p,A}\epsilon, \quad H_{e\text{-}p,O} = \varphi'_{e\text{-}p,O}Q_{\kappa_p}, \tag{3}$$

where ϵ and Q_{κ_p} are the strain and the normal coordinates, respectively. Then the second-order interaction matrix becomes

$$M_{ph\text{-}e\text{-}p} = \sum_l \frac{\langle f|H_{int}|l\rangle\langle l|H_{int}|i\rangle}{E_{e,i} - E_{e,l}} \simeq \sum_l \frac{\langle \psi_f, f^o_{ph}, f^o_p | H_{ph\text{-}e} | \psi_l, f^o_{ph}+1, f^o_p \rangle \langle \psi_l, f^o_{ph}+1, f^o_p | H_{e\text{-}p} | \psi_i, f^o_{ph}+1, f^o_p+1 \rangle}{E_{e,i} - (E_{e,i} - \hbar\omega_p)}, \tag{4}$$

where ψ is the isolated electron wave function, state l is phonon-assisted state, $H_{int}=H_{ph\text{-}e}+H_{e\text{-}p}$ is the interaction Hamiltonian, f^o_{ph} and f^o_p are boson distribution functions. When the above matrix is expanded and plugged into Eq. (1), the transition rates for acoustic and optical phonon-coupled photon absorption become[20,22]

$$\dot{\gamma}_{ph\text{-}e\text{-}p} = \frac{\pi}{2\hbar\epsilon_o}\left(\frac{\varphi^2_{e\text{-}p,A}}{mu_p^2} \text{ or } \frac{\varphi'^2_{e\text{-}p,O}}{m\omega_p^2}\right) \times (s_{ph,i}\cdot\mu_{ph\text{-}e})^2 D_p(E_p)\frac{f^o_p(E_p)}{E_p}e_{ph,i}, \tag{5}$$

where m is the reduced mass of oscillating atom pair, u_p is

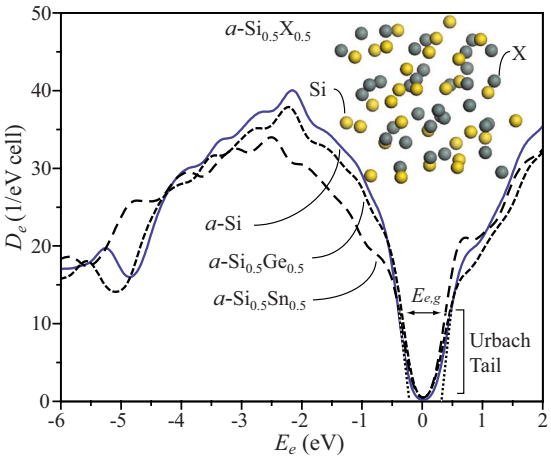

FIG. 3. (Color online) Calculated electron density of states of a-Si, a-$Si_{0.5}Ge_{0.5}$, and a-$Si_{0.5}Sn_{0.5}$ with disordered 64-atom cells generated by the Wooten-Winer-Weaire method (Ref. 11). The band gap $E_{e,g}$ and the Urbach tail are shown. A sample structure of a-$Si_{0.5}X_{0.5}$ is shown as an inset.

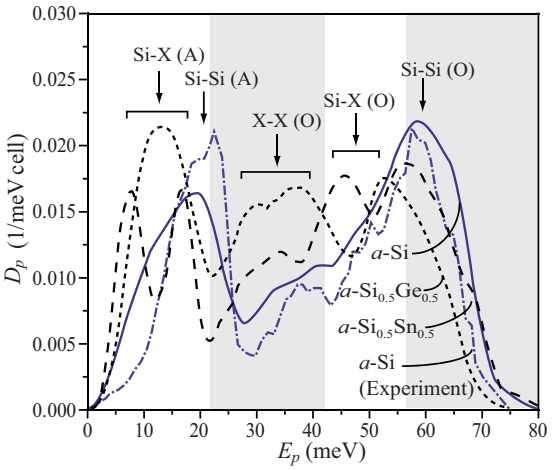

FIG. 4. (Color online) *Ab initio* calculated phonon density of states of a-Si, a-$Si_{0.5}Ge_{0.5}$, and a-$Si_{0.5}Sn_{0.5}$ with disordered 64-atom cells generated by the Wooten-Winer-Weaire method (Ref. 11). The experimental D_p of a-Si using neutron scattering is also shown (Ref. 28).

the speed of sound, ϵ_o is the permittivity, $s_{ph,i}$ is the polarization vector, $\mu_{ph\text{-}e}$ is the electronic transition dipole moment vector, $D_p(E_p)$ is the phonon density of states of phonon having energy E_p, and $e_{ph,i}$ is the energy density of the incoming photon. This transition rate is directly proportional to the absorption coefficient through

$$\sigma_{ph\text{-}e\text{-}p,a} = \frac{\hbar\omega_{ph} n_e \dot{\gamma}_{ph\text{-}e\text{-}p}}{u_{ph} e_{ph,i}} = \frac{\pi\omega_{ph} n_e}{2\hbar u_{ph}\epsilon_o}\left(\frac{\varphi^2_{e\text{-}p,A}}{m u_p^2} \text{ or } \frac{\varphi'^2_{e\text{-}p,O}}{m\omega_p^2}\right) \times (s_{ph,i}\cdot\mu_{ph\text{-}e})^2 D_p(E_p)\frac{f_p^o(E_p)}{E_p}, \quad (6)$$

where n_e is the number density of absorption sites and u_{ph} is the speed of light and the coefficients are theoretically evaluated by *ab initio* calculations or molecular dynamics (MD).[18]

IV. ELECTRONIC STRUCTURE OF a-Si_xX_{1-x}

First, we examine the electronic structure of a-$Si_{1-x}Sn_x$ alloy by calculating the electronic density of states D_e of a-Si with and without X (group-IV elements) using VASP,[23] within the frame work of density functional theory (DFT) and projector augmented wave potentials generated with GGA-PW91 pseudopotential. $4\times4\times4$ Monkhorst-Pack k-point grid was used with energy cutoff of 370 eV. The results are shown in Fig. 3 for a-Si, a-$Si_{0.5}Ge_{0.5}$, and a-$Si_{0.5}Sn_{0.5}$ and one of $Si_{0.5}X_{0.5}$ structure is shown as an inset as an example. Although DFT cannot accurately calculate the excited states and predicts smaller band gaps for insulators and semiconductors,[24,25] we can still examine the effect of X near the band gap within the same structure. The results clearly show a band gap $E_{e,g}$ of approximately 0.58 eV (which is similar to that of c-Si predicted by DFT and smaller compared to a-Si:H due to no H content) and the Urbach tail states indicating mostly four coordination. For such small cell sizes, defect states due to dangling bonds are not evident. However, the defect states are not relevant for the scope of this study. The comparison of the D_e show that even with high X content, the overall density distribution near the band edge is virtually unchanged. This is because most of the electronic density is known to be composed of s and p orbitals near the band gap[26] which is retained in the a-$Si_{1-x}X_x$ alloy (X being a group-IV element). The results indicate that D_e is not sensitive to the type of the element but on the coordination of the atoms. However, for Sn, the results indicate a smaller band gap which may be advantageous in increasing the energy conversion efficiency where the ideal single junction band gap is found to be approximately 1.1 eV (Ref. 1) whereas band gap for a-Si:H is approximately 1.7 eV.

V. PHONON DENSITY OF STATES OF a-Si_xX_{1-x}

We perform *ab initio* phonon calculation of this 64-atom a-Si cell using CASTEP.[27] Finite displacement method with GGA-PW91 pseudopotential are used along with $2\times2\times2$ k-point grid and energy cutoff of 200 eV. Figure 4 shows calculated D_p of a-Si, a-$Si_{0.5}Ge_{0.5}$, and a-$Si_{0.5}Sn_{0.5}$ using 0.5 THz smearing, along with the experimental neutron-scattering result of a-Si. The *ab initio* phonon peaks of the a-Si is in good agreement with the experiment near 25 (A) and 60 meV (O). When element X is added, the lower phonon energy peaks (due to Si-X and X-X) appear. For a-$Si_{0.5}Ge_{0.5}$, there are no distinguished peaks near 15 and 55 meV, indicating mixed phonon states between the Si and Ge acoustic and optical oscillating modes and this trend is also found in the Raman experiment and MD simulation results.[28] However, a strong Ge-Ge optical mode peak is found near 37 meV. For a-$Si_{0.5}Sn_{0.5}$, due to significant mismatch between the two elements, large segregation of the phonon peaks are found. The Si-Sn and Sn-Sn optical-phonon peaks are near

45 and 30 meV. As the phonon peak energy decreases, the occupation probability of these modes increase (due to boson function) which predict enhancement of the phonon-coupled photon absorption and the overall absorption coefficient. Unlike D_e, D_p shows significant dependence on the alloying element, indicating that the phonon spectrum is readily altered by composition. Experiments taking advantage of these trends are found in laser cooling of glasses (amorphous), varying the composition to enhance the cooling performance.[29,30]

VI. PHONON-COUPLING ENHANCED ABSORPTION AND CURRENT DENSITY

We now assess the increased current generation due to increased absorption using the following, ideal current-density generation equation under illumination within the limits of the hemispherical solid angle:[1]

$$j_e = e_c \int_{E_{ph}>E_{e,g}}^{\infty} [1-\rho_r(E_{ph})]\{1-\exp[-\sigma_{ph\text{-}e\text{-}p,a}(E_{ph})L]\} \times \frac{\pi I_{ph}(E_{ph},T)dE_{ph}}{\hbar\omega_{ph}}, \tag{7}$$

where e_c is the electron charge, $\rho_r(E_{ph})$ is the spectral reflectivity, $\sigma_{ph\text{-}e\text{-}p,a}(E_{ph})$ is the absorption coefficient due to phonon-coupled photon absorption, L is the optical length, and $I_{ph}(E_{ph},T)$ is the spectral intensity of the sun (approximated as blackbody). The optically thin limit gives $1-\exp[-\sigma_{ph\text{-}e\text{-}p,a}(E_{ph})L] \simeq \sigma_{ph,a}(E_{ph})L$.[18,31] Now, to assess the current-density generation improvement using enhanced phonon-coupled process using alloy element X, we use a scaled total current-density generation equation

$$j_e^* = \sum j_{e,n}^* = \sum \frac{j_{e,n}(a\text{-}Si_{1-x}X_x)}{j_{e,n}(a\text{-}Si)} = \sum \frac{\int_{E_{ph}>E_{e,g}}^{\infty} \sigma_{ph\text{-}e\text{-}p,a}(a\text{-}Si_{1-x}X_x) I_{ph}(E_{ph},T)dE_{ph}}{\int_{E_{ph}>E_{e,g}}^{\infty} \sigma_{ph\text{-}e\text{-}p,a}(a\text{-}Si) I_{ph}(E_{ph},T)dE_{ph}}, \tag{8}$$

where $j_{e,n}^*$ is the normalized current for peak phonon energies, $j_{e,n}(a\text{-Si})$ is the current generated by acoustic and optical-phonon peaks of a-Si. We assume that ρ_r and L remain the same over the entire solar spectrum. Then, this normalized current density depends only on the absorption coefficient and the spectral intensity. Now, using Eq. (6) and the validated assumption that the electronic structure near the band gap does not change with alloyed X, all the quantum quantities related to electron-photon interaction cancels and the normalized current becomes

$$j_e^* = \sum \frac{\int_{E_{ph}>E_{e,g}}^{\infty} \left[\left(\frac{\varphi_{e\text{-}p,A}^2}{mu_p^2} \text{ or } \frac{\varphi_{e\text{-}p,O}'^2}{m\omega_p^2}\right)\frac{D_p(E_p)f_p^o(E_p)}{E_p}\right]_{a\text{-}Si_{1-x}X_x} I_{ph}(E_{ph},T)dE_{ph}}{\int_{E_{ph}>E_{e,g}}^{\infty} \left[\left(\frac{\varphi_{e\text{-}p,A}^2}{mu_p^2} \text{ or } \frac{\varphi_{e\text{-}p,O}'^2}{m\omega_p^2}\right)\frac{D_p(E_p)f_p^o(E_p)}{E_p}\right]_{a\text{-}Si} I_{ph}(E_{ph},T)dE_{ph}}, \tag{9}$$

which is only dependent on the acoustic and optical phonon-coupling related quantities integrated over the solar spectrum.

The electron-phonon couplings $\varphi_{e\text{-}p,A}$ and $\varphi'_{e\text{-}p,O}$ are the electronic energy changes caused by the bond displacements of phonon modes and here we use the theory of harmonic oscillators. The stretching mode frequency is $\omega_p=(\Gamma/m)^{1/2}$, where Γ is the equivalent force constant found using the combinative rule and monatomic bond properties[20,32,33] and m is the reduced mass. Then the energy change by displacement $\Delta_p=(\hbar/2m\omega_p)^{1/2}$ becomes $\varphi_{e\text{-}p,A} \equiv 0.5\Gamma\Delta_p^2$. For the optical phonons the energy change is defined over the bond length as $\varphi'_{e\text{-}p,O} \equiv 0.5\Gamma\Delta_p^2/r_e$, where r_e is equilibrium bond length (i.e., Si-Si, Si-X, and X-X). Then Eq. (9) becomes

$$j_e^* = \sum \frac{\int_{E_{ph}>E_{e,g}}^{\infty} \left[\left(\frac{\hbar^2\Gamma^{1/2}}{u_p^2 m^{3/2}} \text{ or } \frac{\hbar^2}{m^{1/2}r_e^2\Gamma^{1/2}}\right)D_p(E_p)f_p^o(E_p)\right]_{a\text{-}Si_{1-x}X_x} I_{ph}(E_{ph},T)dE_{ph}}{\int_{E_{ph}>E_{e,g}}^{\infty} \left[\left(\frac{\hbar^2\Gamma^{1/2}}{u_p^2 m^{3/2}} \text{ or } \frac{\hbar^2}{m^{1/2}r_e^2\Gamma^{1/2}}\right)D_p(E_p)f_p^o(E_p)\right]_{a\text{-}Si} I_{ph}(E_{ph},T)dE_{ph}}. \tag{10}$$

The normalized, peak generated current density showing the phonon-coupling enhanced absorption, for a-$Si_{0.5}Ge_{0.5}$ and a-$Si_{0.5}Sn_{0.5}$ as a function of the phonon energy, are presented in Fig. 5. The peak phonon energies used are those in Fig. 4. The net current which is the summation over all peak phonon energies is also shown (and indicated as net enhancement). The results show that the current generation is significantly increased due to the Si-X and X-X optical phonon-coupled absorption (high absorption rate at lower phonon energies and larger D_p). However, for the acoustic and Si-Si optical

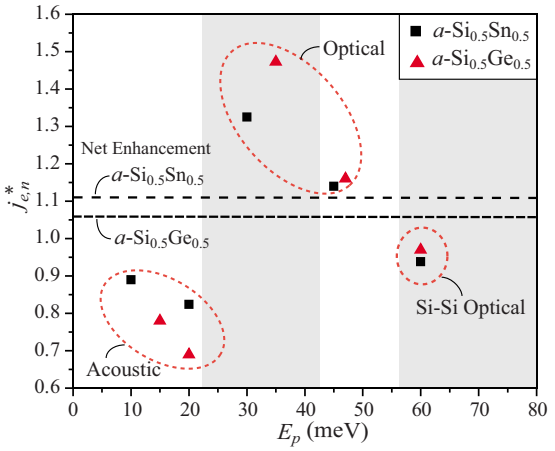

FIG. 5. (Color online) Normalized phonon-coupled current density using the peak phonon energies of a-$Si_{0.5}Ge_{0.5}$ and a-$Si_{0.5}Sn_{0.5}$. The scaled total phonon-coupled current density is shown as net enhancement using broken lines.

phonon-coupled absorption, there is a reduction in the current. a-$Si_{0.5}Ge_{0.5}$ shows a larger degradation for the acoustic modes, compared to that of a-$Si_{0.5}Sn_{0.5}$ (because of the small shift in the peak due to mixed phonon states). Degradation at the Si-Si optical mode is alleviated due to higher electron-phonon coupling. Although a-$Si_{0.5}Ge_{0.5}$ shows larger enhancement of the optical-phonon-coupled absorption, when the reduced acoustic and Si-Si optical coupled absorptions are included, a-$Si_{0.5}Sn_{0.5}$ shows a higher net current j_e^* enhancement of approximately 11%. The trend for the optical phonon-coupled current generation shows the combined effect of $\Gamma^{-1/2}$ and f_p^o dependence in Eq. (10), favoring low-energy optical-phonon modes. The higher enhancement associated with a-$Si_{0.5}Ge_{0.5}$ in this regime is due to high $\varphi'_{e\text{-}p,O}$ and D_p. The current generation due to the acoustic modes show similar behavior but the f_p^o dependence is reduced (due to $\Gamma^{1/2}$ dependence). Therefore, alloys with low-energy optical phonons enhance the absorption and efficiency of solar-energy conversion.

VII. EFFECTS ON CARRIER TRANSPORT

We now address the carrier transport properties which is related to the collection efficiency. Unlike c-Si, transport kinetics in a-Si are more complex and several theories have been proposed[2] and here we address them qualitatively and assess the dominant scattering mechanism. The total electron-scattering rate, τ_e^{-1} is expressed as a combination of various scattering mechanisms through Matthiessen rule as

$$\frac{1}{\tau_e} = \frac{1}{\tau_{i,im}} + \frac{1}{\tau_a} + \frac{1}{\tau_{n,im}} + \frac{1}{\tau_{c\text{-}c}} + \frac{1}{\tau_{p,A}} + \frac{1}{\tau_{p,O}}, \tag{11}$$

where $\tau_{i,im}^{-1}$, τ_a^{-1}, $\tau_{n,im}^{-1}$, and $\tau_{c\text{-}c}^{-1}$ are ionized impurity, alloy, neutral impurity, and carrier-carrier scattering, respectively. $\tau_{p,A}^{-1}$ and $\tau_{p,O}^{-1}$ are the acoustic and optical-phonon scattering. The ionized impurity scattering rate shows temperature dependence of $T^{-3/2}$ so, any increase ionized impurity due to Sn alloying is expected to be negligible at operating temperatures of SPV. Alloy scattering rate is highly dependent on cluster size and show $T^{1/2}$ dependence.[34] For a-$Si_{1-x}Sn_x$, the cluster size dependence is not relevant when uniform distribution of the alloy is assumed. Carrier-carrier scattering rate is also negligible for carrier concentrations of less than 10^{17} cm^{-3} and the effects decreases as film thickness is reduced.[2] Similar to phonon-coupled absorption, acoustic phonon scattering is expected to be lower for Ge and Sn alloyed a-Si, however, higher optical-phonon scattering is expected due to enhancement of Si-X and X-X oscillation modes and this issue needs to be further addressed. Still phonon scattering can be alleviated by predicted increased absorption that allows for thinner films which, in turn, reduce the amount of materials used.

VIII. CONCLUSIONS

We have expanded the second-order interaction matrix using the weak-phonon-coupled state approximation and the isolated electron representation (noting the covalent nature and the disorder phase of the amorphous semiconductors). We predict that alloying with Ge or Sn increases phonon-coupled photon absorption and enhances the current generation near the optical band edge for a-Si. The D_e calculations show that the electronic band gap is not significantly altered for up to 50% alloying. However, due to the lower force constant and higher mass mismatch, the phonon spectrum shows significant redshifting of peaks resulting from Si-Sn (or Ge) and Sn-Sn (or Ge-Ge) vibrations. These shifted optical-phonon energies result in higher phonon occupation, thus enhancing the phonon-coupled absorption. Therefore, this soft-bond alloying of a-Si results in net phonon-coupling enhanced absorption suitable for solar photovoltaics. Synthesis by nonequilibrium processes such as ultrafast laser melting of laminates, makes this finding promising. Addition of Sn may also help with long-term stabilization of the amorphous Si SPV films, which has been a concern.[35]

ACKNOWLEDGMENTS

We thank David Drabold for the a-Si atomic coordinates and Steve Yalisove and John Kieffer for fruitful discussions. Also we are grateful for the financial support by NSF (Thermal Transport and Processes) and DOE (Center for Solar and Thermal Energy Conversion, University of Michigan).

*kaviany@umich.edu

[1] A. Luque and S. Hegedus, *Handbook of Photovoltaic Science and Engineering* (Wiley, West Sussex, 2003).

[2] R. Street, *Hydrogenated Amorphous Silicon* (Cambridge University Press, Cambridge, 1991).

[3] Y. Pan, F. Inam, M. Zhang, and D. A. Drabold, Phys. Rev. Lett. **100**, 206403 (2008).

[4] D. A. Drabold, P. A. Fedders, S. Klemm, and O. F. Sankey, Phys.

Rev. Lett. **67**, 2179 (1991).
[5] J. Dong and D. A. Drabold, Phys. Rev. B **54**, 10284 (1996).
[6] J. Dong and D. A. Drabold, Phys. Rev. Lett. **80**, 1928 (1998).
[7] J. Kim and M. Kaviany, Appl. Phys. Lett. **95**, 074103 (2009).
[8] J. Kouvetakis, J. Menendez, and A. V. G. Chizmeshya, Annu. Rev. Mater. Res. **36**, 497 (2006).
[9] P. Moontragoon, Z. Ikonic, and P. Harrison, Semicond. Sci. Technol. **22**, 742 (2007).
[10] A. J. H. McGaughey, M. I. Hussein, E. S. Landry, M. Kaviany, and G. M. Hulbert, Phys. Rev. B **74**, 104304 (2006).
[11] F. Wooten, K. Winer, and D. Weaire, Phys. Rev. Lett. **54**, 1392 (1985).
[12] A. Poruba, J. Springer, L. Mullerova, A. Beitlerova, M. Vanecek, N. Wyrsch, and A. Shah, J. Non-Cryst. Solids **338-340**, 222 (2004).
[13] Y. P. Varshni, Physica (Amsterdam) **34**, 149 (1967).
[14] F. Mott and E. A. Davis, *Electronic Processes in Non-Crystalline Materials* (Oxford University Press, New York, 1979).
[15] G. D. Cody, *Hydrogenated Amorphous Silicon, Part B, Optical Properties*, Semiconductors and Semimetals Vol. 21 (Academic Press, New York, 1984).
[16] K. Fukutani, M. Kanbe, W. Futako, B. Kaplan, T. Kamiya, C. Fortmann, and I. Shimizu, J. Non-Cryst. Solids **227-230**, 63 (1998).
[17] C. M. Fortmann, Phys. Rev. Lett. **81**, 3683 (1998).
[18] M. Kaviany, *Heat Transfer Physics* (Cambridge University Press, Cambridge, 2008).
[19] X. L. Ruan and M. Kaviany, J. Comput. Theor. Nanosci. **5**, 221 (2008).
[20] J. Kim, A. Kapoor, and M. Kaviany, Phys. Rev. B **77**, 115127 (2008).
[21] J. Fernández, A. Mendioroz, A. J. García, R. Balda, and J. L. Adam, Phys. Rev. B **62**, 3213 (2000).
[22] X. L. Ruan and M. Kaviany, Phys. Rev. B **73**, 155422 (2006).
[23] G. Kresse and J. Furthmüller, Phys. Rev. B **54**, 11169 (1996).
[24] D. R. Hamann, Phys. Rev. Lett. **42**, 662 (1979).
[25] G. B. Bachelet and N. E. Christensen, Phys. Rev. B **31**, 879 (1985).
[26] R. Biswas, C. Z. Wang, C. T. Chan, K. M. Ho, and C. M. Soukoulis, Phys. Rev. Lett. **63**, 1491 (1989).
[27] M. D. Segall, P. J. D. Lindan, M. J. Probert, C. J. Pickard, P. J. Hasnip, S. J. Clark, and M. C. Payne, J. Phys.: Condens. Matter **14**, 2717 (2002).
[28] A. M. Bouchard, R. Biswas, W. A. Kamitakahara, G. S. Grest, and C. M. Soukoulis, Phys. Rev. B **38**, 10499 (1988).
[29] J. Thiede, J. Distel, S. R. Greenfield, and R. I. Epstein, Appl. Phys. Lett. **86**, 154107 (2005).
[30] M. Sheik-Bahae and R. I. Epstein, Nat. Photonics **1**, 693 (2007).
[31] K. Driss-Khodja, A. Gheorghiu, and M.-L. Theye, Opt. Commun. **55**, 169 (1985).
[32] B. L. Huang and M. Kaviany, J. Appl. Phys. **100**, 123507 (2006).
[33] B. Henderson and G. F. Imbusch, *Optical Spectroscopy of Inorganic Solids* (Clarendon Press, Oxford, 1989).
[34] J. Singh, *Electronic and Optoelectronic Properties of Semiconductor Structures* (Cambridge University Press, Cambridge, 2003).
[35] D. Staebler and C. Wronski, Appl. Phys. Lett. **31**, 292 (1977).